Redox Biology 14 (2018) 566–575

Contents lists available at ScienceDirect

Redox Biology

journal homepage: www.elsevier.com/locate/redox

Research paper

A single cysteine post-translational oxidation suffices to compromise globular proteins kinetic stability and promote amyloid formation

Patrizia Marinelli[a,1], Susanna Navarro[a,1], Ricardo Graña-Montes[a], Manuel Bañó-Polo[a], María Rosario Fernández[a], Elena Papaleo[b], Salvador Ventura[a,*]

[a] Institut de Biotecnologia i de Biomedicina and Departament de Bioquímica i Biologia Molecular, Universitat Autònoma de Barcelona, 08193 Bellaterra, Barcelona, Spain
[b] Computational Biology Laboratory, Danish Cancer Society Research Center, 2100 Copenhagen, Denmark

ARTICLE INFO

Keywords:
Protein oxidation
Protein misfolding
Protein aggregation
Oxidative stress
Post-translational modification

ABSTRACT

Oxidatively modified forms of proteins accumulate during aging. Oxidized protein conformers might act as intermediates in the formation of amyloids in age-related disorders. However, it is not known whether this amyloidogenic conversion requires an extensive protein oxidative damage or it can be promoted just by a discrete, localized post-translational modification of certain residues. Here, we demonstrate that the irreversible oxidation of a single free Cys suffices to severely perturb the folding energy landscape of a stable globular protein, compromise its kinetic stability, and lead to the formation of amyloids under physiological conditions. Experiments and simulations converge to indicate that this specific oxidation-promoted protein aggregation requires only local unfolding. Indeed, a large scale analysis indicates that many cellular proteins are at risk of undergoing this kind of deleterious transition; explaining how oxidative stress can impact cell proteostasis and subsequently lead to the onset of pathological states.

1. Introduction

Protein misfolding and aggregation are linked to the onset of more than 40 human diseases, including neurodegenerative disorders such Alzheimer's, Parkinson's and prion diseases or amyotrophic lateral sclerosis (ALS), but also non-neurodegenerative pathologies like type II diabetes, cardiomyopathies, cataracts or even certain types of cancer [1,2].

Native state stability and folding cooperativity disfavour the aggregation of globular proteins, because they prevent local or global unfolding and the subsequent population of aggregation-prone intermediates. This appears as a very successful evolutionary strategy to avoid aggregation, since only a few globular proteins aggregate from their native conformation under physiological conditions [3]. Accordingly, conformational diseases where globular proteins are involved, are often triggered by pathogenic mutations that destabilize the native fold, thus facilitating subsequent aggregation [4,5]. Even conservative mutations might shift the delicate equilibrium between the folded and aggregation-prone states in the cell [6], because increased conformational fluctuations suffice to enable the aggregation reaction, without a need for global unfolding [7].

During their biological lifetime, proteins are frequently subject of irreversible non-enzymatic post-translational modifications (PTM) associated to molecular aging. Oxidation represents an important class of non-enzymatic PTMs since cells produce significant levels of reactive oxygen species (ROS) [8], which can react with susceptible side chains, inducing various chemical modifications. Similarly to mutations, these modifications may cause misfolding and shift the conformational equilibrium towards more aggregation-prone states. Indeed, oxidative protein damage is being found associated with an increasing number of diseases and with aging [9–11].

The thiol functional group of Cys is particularly sensitive to redox conversion and the thiol group of cysteines can be oxidized to different states. The thiol and disulfide forms are the most common, but derivatives with a higher oxidation state such as sulfenic (RSOH), sulfinic (RSO_2H), and sulfonic (RSO_3H) acid are being detected in a growing number of proteins. Indeed, up to a 5% of cellular protein Cys occur in the sulfinic or sulfonic acid form [12]. Sulfonic acid is the most highly oxidized species of thiols and its formation is irreversible. We have still little information on how site-specific cystein sulfonic acid ($CySO_3H$)

Abbreviations: PTM, post-translational modifications; ROS, reactive oxygen species; MSO, methionine sulfoxide; CD, circular dichroism; MD, molecular dynamics; Th-T, thioflavin T; CR, Congo red

* Correspondence to: Institut de Biotecnologia i de Biomedicina, Parc de Recerca UAB, Mòdul B, Universitat Autònoma de Barcelona, E-08193 Bellaterra, Barcelona, Spain.
E-mail address: salvador.ventura@uab.es (S. Ventura).
[1] These authors contributed equally to this work.

https://doi.org/10.1016/j.redox.2017.10.022
Received 31 July 2017; Received in revised form 24 October 2017; Accepted 29 October 2017
Available online 31 October 2017
2213-2317/ © 2017 The Authors. Published by Elsevier B.V. This is an open access article under the CC BY-NC-ND license (http://creativecommons.org/licenses/BY-NC-ND/4.0/).

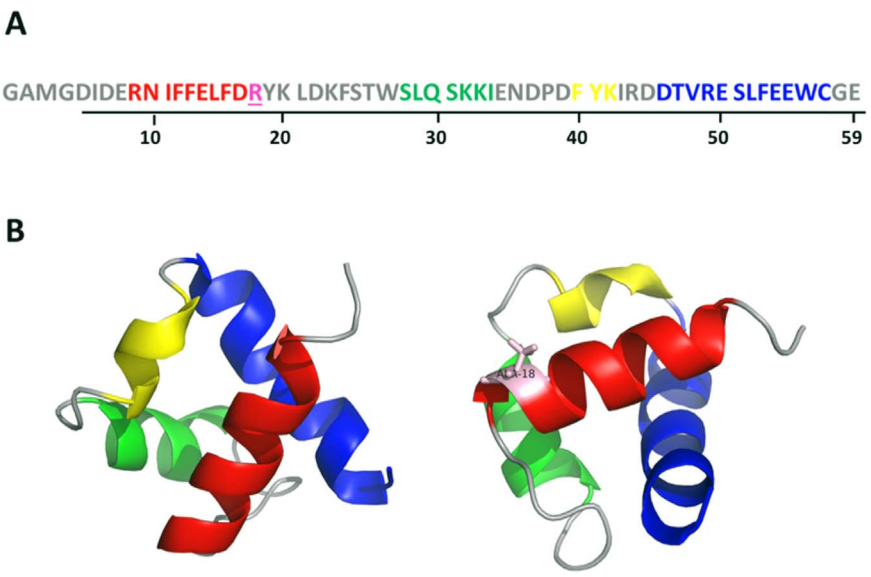

Fig. 1. *Primary and tertiary structures of the URN1 FF domain.* (A) Amino acidic sequence and (B) ribbon representation of FF-WT (left) and FF-R18A mutant (right) are shown. Colored regions correspond to: α-helix 1 (red), α-helix 2 (green), helix 3_{10} (yellow) and α-helix 3 (blue). The mutated residue (Arg18Ala) is represented in pink. The Protein Data Bank accession code for the WT structure is 2JUC. The underlined residues correspond to the natural FF domain. This figure was prepared with PyMOL (www.pymol.org).

formation may impact protein conformation. Here, we take advantage of the single Cys residue in position 57 of the yeast URN1 FF domain to gain molecular insights on the effect of such PTM in the folding and aggregation landscapes of this model globular protein.

FF domains are small protein-protein interaction modules consisting of ~50–70 residues and characterized by the presence of two conserved Phe residues at their N- and C-termini [13]. This fold consists of three α-helices arranged as an orthogonal bundle with a 3_{10} helix in the loop connecting the second and the third helices [14,15] (Fig. 1). FF domains are involved in RNA splicing, signal transduction and transcription processes [16,17], they are present in a variety of eukaryotic nuclear transcription and splicing factors, and their sequences are well conserved from yeast to humans [13]. The folding and aggregation landscapes of several of these domains, including the URNF1 FF domain, have been characterized in detail [18–21]. This provides a unique opportunity to dissect the impact of selective post-translational Cys oxidation on protein folding kinetics, thermodynamic stability and aggregation propensity. Here, we integrate experimental and computational analyses to understand how these properties are affected in this model protein as well as at the proteome level. Overall, our results demonstrate that the irreversible oxidation of a single free Cys is able to dramatically impact the folding and stability of a globular protein, leading to its aggregation into amyloid-like structures under physiological conditions. Moreover, the data suggest that a significant fraction of cellular proteins are exposed to this particular risk.

2. Material and methods

2.1. URN1 FF cloning, expression and purification

FF domain of yeast URN1 protein corresponding to residues 212-266 was cloned, expressed and purified as previously described [14]. The purity of the samples was checked by SDS-PAGE. Protein concentration was determined by UV absorption using an $\varepsilon_{280\ nm}$ value of 1.948 $mg^{-1}\,mL\,cm^{-1}$. FF mutants were engineered by PCR with QuikChangeII Site-directed Mutagenesis Kit, by following the manufacturer instructions (Agilent Technologies). Unless otherwise noted, all the experiments were carried out in 50 mM sodium acetate buffer at pH 5.7.

2.2. FoldX modelling

URN1-FF mutant models were built using the BuildModel command / routine of the FoldX algorithm [22] (version 3b6) on top of the FF-WT structure (PDB: 2JUC). The resultant structures were used to calculate the effect of the mutation on protein stability ($\Delta\Delta G = \Delta G_{mut} - \Delta G_{wt}$) [23].

2.3. Sample oxidation

Oxidation of FF domains was attained by incubating 1 mg/mL protein in presence of 5% v/v H_2O_2 solution for 12 h at 298 K. An extensive water dialysis at 277 K was used to remove non-reacted H_2O_2 from the protein solution before lyophilization. The oxidation state of the sample was analyzed on an UltrafleXtreme mass spectrometer (Bruker Daltonics) before or after triptic digestion (3 h at 37 °C). Free Cys residues were alkylated by adding to the samples an excess of 75 mM iodoacetamide in 50 mM ammonium bicarbonate buffer, pH = 8. The reaction was allowed to proceed for 30 min at room temperature.

2.4. Circular dichroism, Trp intrinsic fluorescence and bis-ANS binding

Lyophilized proteins were dissolved at 20 μM in 50 mM sodium acetate at pH 5.7, filtered through a 0.22 μm filter and immediately analyzed. Far-UV CD spectra were recorded from 260 to 200 nm, at 0.2 nm intervals, 1 nm bandwidth and a scan speed of 100 nm/min in a Jasco-715 spectropolarimeter (Jasco Corporation, Japan) thermostated at 298 K. Twenty accumulations were averaged for each spectrum. Trp intrinsic fluorescence was analyzed at 298 K in a Jasco FP8200 spectrofluorometer (Jasco Corporation, Japan). Three averaged spectra were accumulated using an excitation wavelength of 280 nm and recording the emission from 300 to 400 nm with slit widths of 5 nm. To study the binding to 4,4′-dianilino-1,1′- binaphthyl-5,5′-disulfonic acid (bis-ANS), protein solutions were prepared at 20 μM in presence of 10 μM bis-ANS and analyzed immediately. Three spectra were recorded in a Jasco FP8200 spectrofluorometer (Jasco Corporation, Japan) using an excitation wavelength of 370 nm and an emission between 400 and 600 nm with slit widths of 5 nm.

2.5. Thermal and chemical denaturation

Protein samples were dissolved at 20 μM to study thermal stabilities by far-UV CD and Trp intrinsic fluorescence intensity. The ellipticity at 222 nm was registered in a Jasco-715 spectropolarimeter (Jasco Corporation, Japan) in a range from 273 to 363 K, each 0.1 K with 2 min of temperature equilibrium between measures. Trp intrinsic fluorescence emission was recorded at 360 nm after excitation at

280 nm, using slit widths of 5 nm for both wavelengths in a Jasco FP8200 spectrofluorometer (Jasco Corporation, Japan). The fluorescence emission was monitored each 0.5 K with 1 min of temperature equilibrium between measures.

For chemical denaturation, samples were prepared at 20 μM in presence of different concentrations of denaturant agent (0–9 M of urea). The reaction was left to equilibrate for 20 h at room temperature and analyzed by CD and Trp intrinsic fluorescence at 222 nm and 280/360 nm (ex/em), respectively. The results were fitted to a two-state transition curve where the signals of the folded and unfolded states are dependent on the temperature/denaturant concentration using the nonlinear least squares algorithm provided with Kaleidagraph (Synergy Software).

2.6. NMR spectroscopy

Lyophilized proteins were prepared at 50 μM in 20 mM deuterated sodium phosphate buffer and 130 mM NaCl, at pH 5.7, using a 9:1H_2O/D_2O ratio. One-dimensional NMR spectra were accumulated at specific temperatures on a Bruker AVANCE 600-MHz spectrometer using solvent suppression WATERGATE techniques. The collected spectra were processed and analyzed using the TopSpinv2.0 software packages from (Bruker Biospin).

2.7. Folding and unfolding kinetics parameters

Folding and unfolding kinetics were followed by recording intrinsic fluorescence changes upon transition at 298 K in a Bio-Logic SFM-3 stopped-flow instrument (Bio-Logic Science Instruments), employing an excitation wavelength of 280 nm and a 320 nm emission cut-off filter. The protein concentration was 20 μM in 50 mM sodium acetate at pH 5.7 with or without urea. All fluorescence traces fitted well to a single exponential function, and kinetic parameters were derived to a two-state folding model, using the Kaleidagraph version 4.0 (Synergy Software), as previously described [18].

2.8. Molecular dynamics (MD) simulations

MD simulations were carried as described in the Supplementary Material.

2.9. Aggregation kinetics

Lyophilized URN1-FF samples were prepared at 100 μM in sodium acetate buffer at pH 5.7 in presence of 25 μM of Thioflavine T (Th-T). After equilibrating during 5 min at 310 K, Th-T fluorescence intensity was monitored during 60 min in a Jasco FP8200 spectrofluorometer (Jasco Corporation, Japan) using the Th-T excitation and emission wavelengths at 440 and 475 nm, respectively, with slit widths of 5 nm.

2.10. Structural analysis of protein aggregates

Lyophilized protein samples were prepared at 50 μM in sodium acetate buffer at pH 5.7 and incubated at 310 K under agitation during one week.

Aggregated samples were diluted to 10 μM in sodium acetate buffer at pH 5.7 in presence of 25 μM of Th-T and analyzed in a Jasco FP8200 spectrofluorometer (Jasco Corporation, Japan). Three Th-T spectra were accumulated exciting at 440 nm and acquiring fluorescence emission between 460 and 600 nm with excitation and emission slit widths of 5 nm. In Congo red (CR) binding assay, FF domain aggregates were diluted to 10 μM in presence of 20 μM of CR and optical absorption spectra were recorded from 400 to 700 nm at 298 K. Each trace was the average of 3 accumulated spectra in a Cary-400 UV/Vis spectrophotometer (Varian Inc.). Spectra of protein only and CR solution were acquired to subtract protein scattering and dye contribution.

Aggregated FF domains solutions, diluted at 10 μM, were also analyzed by far-UV CD and bis-ANS dye binding as described above.

2.11. Transmission Electron Microscopy (TEM)

Aggregated samples were diluted tenfold in water and 10 μL were placed on carbon-coated copper grids during 5 min. The grids were then washed with distilled water and stained with 2% (w/v) uranyl acetate for 1 min. An HITACHI H-7000 transmission electron microscope operating at an accelerating voltage of 75 kV was used to visualize fibrils.

3. Results

3.1. FF domain oxidation specifically converts Cys57 into a cysteine sulfonic acid

To investigate whether the impact of oxidation on protein properties is modulated by the native state stability, we used here two different FF domains: the wild type domain (FF-WT) and an Arg18Ala mutant (FF-R18A) (Fig. 1), which corresponds to a destabilized, yet natively folded FF domain variant.

FF domains were incubated in the presence of H_2O_2 and their oxidation state was analyzed by mass spectrometry (MS). An increase of ≈ 64 Da was observed for both oxidized proteins, suggesting the incorporation of 4 oxygen atoms (supplementary Fig. 1). Further tryptic digestion coupled with MS analysis allowed the identification of two specific oxidation sites at Met3 and Cys57 (supplementary Table 1). A methionine sulfoxide (MSO) accounting for one extra oxygen atom and a cysteine sulfonic acid ($CySO_3H$) incorporating 3 new oxygen atoms (≈ +48 Da) were detected in the oxidized states of both FF variants. Upon iodoacetamide treatment, carboxyamidomethyl Cys (CAM ≈ +57 Da) formation is observable only for peptides derived from non-oxidized proteins, consistent with the presence of a free and accessible Cys57 thiol group in their native structures (supplementary Table 1). In contrast, the Cys57 sulfonic acid in the oxidized domains prevents the alkylation reaction. Therefore, the H_2O_2-induced FF oxidation resulted in the modification of only two residues. Cys57 is located in the α-helix 3, whereas Met3 is absent in the natural domain, placed in the disordered N-terminal tail and, according to the NMR solution structure [14], not interacting with any other protein residue. Therefore, any impact on the protein globular conformation due to oxidation can be adscribed to $CysSO_3H$ formation at position 57.

3.2. Conformational characterization of oxidized FF domains

The conformational properties of non-oxidized (FF-WT and FF-R18A) and oxidized proteins (FF-WT-OX and FF-R18A-OX) were studied at 20 μM concentration, pH 5.7 at 298 K, by far-UV CD spectroscopy (Fig. 2A), Trp intrinsic fluorescence (Fig. 2B) and bis-ANS binding (Fig. 2C). In these conditions the URNF1 FF domain exhibits maximal stability and solubility [18]. The typical α-helical minima at 210 and 222 nm, together with a characteristic FF domain minimum at 230 nm, are observed in the CD spectra of both non-oxidized proteins. The FF-WT-OX domain retains the native secondary structure spectrum. In contrast, the FF-R18A-OX spectrum reveals a conversion towards a largely disordered conformation, displaying a minimum at ≈ 205 nm (Fig. 2A).

The FF domain has two Trp residues at position 27 and 56 and their fluorescence is a sensitive probe of the FF domain native structure [18]. The FF-WT-OX Trp emission spectrum shows higher fluorescence intensity compared with that of the FF-WT, but keeps the same emission maximum, indicating a larger exposure of Trp residues in a native-like environment (Fig. 2B). The fluorescence spectrum of FF-R18A-OX is significantly red-shifted and displays a higher maximum than that of the non-oxidized mutant, consistent with the observed changes in secondary structure and likely associated with the opening of the globular

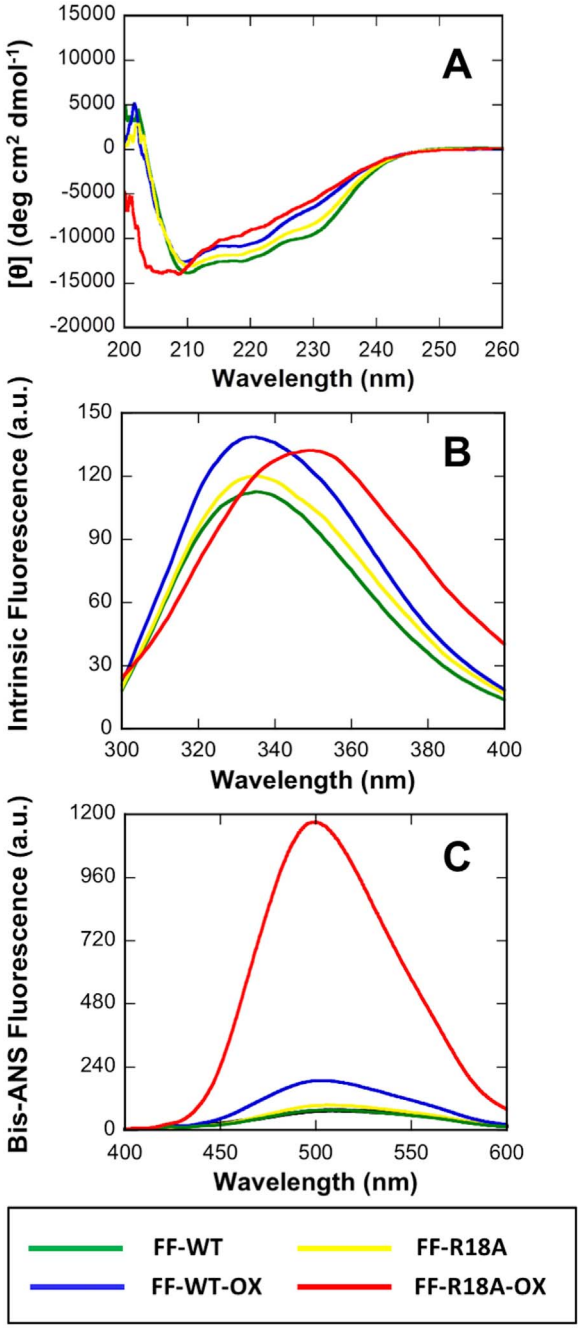

Fig. 2. *Conformational properties of oxidized and non-oxidized FF domains.* FF domains were analyzed using (A) far-UV CD spectroscopy, (B) Trp intrinsic fluorescence and (C) bis-ANS fluorescence, at 298 K. Free bis-ANS emission spectrum is represented with a black line.

structure and the concomitant exposure of hydrophobic regions, as indicated by the high enhancement of bis-ANS fluorescence in its presence (Fig. 2C). The analysis of bis-ANS binding also confirms conformational changes occurring in FF-WT-OX, but they are much smaller than in FF-R18A-OX. The one-dimensional NMR (^{1}H-NMR) spectra of the oxidized FF domains at 298 K shows, in both cases, an alteration of the native signal dispersion and peak sharpness suggesting structural rearrangements relative to the parental proteins (supplementary Fig. 2).

3.3. Impact of Cys57 oxidation on FF domain stability

Thermal unfolding of the FF domains was followed at pH 5.7 by far-UV CD and Trp intrinsic fluorescence, monitoring the changes in molar ellipticity and fluorescence emission at 222 and 360 nm, respectively (Fig. 3). The thermal denaturation curves show a single cooperative transition and the data could be fitted to a two-state unfolding model for all analyzed FF domains except for FF -R18A- OX, due to its lower thermostability.

The stability of both FF domains resulted considerably perturbed by $CySO_3H$ formation (Fig. 3A and B), with a decrease in FF-WT-OX T_m of $\approx$ 20 K respect that of FF-WT, and a reduction $>$ 20 K in the case of the R18A-OX-T_m relative to FF-R18A (supplementary Table 2). These data were corroborated by thermal denaturation followed by H-NMR[1]. Reduction of the native signal dispersion is observed at lower temperatures in oxidized than in non-oxidized species both for FF-WT and FF-R18A (supplementary Fig. 2). In all cases the reaction was reversible.

The chemical unfolding of the FF domains was analyzed at pH 5.7 and 298 K. The urea denaturation curves at equilibrium were obtained recording the changes in molar ellipticity at 222 nm (Fig. 3C) and Trp intrinsic fluorescence at 360 nm (Fig. 3D) at increasing denaturant concentrations. The thermodynamic values were calculated assuming a two-state model according to the unfolding single cooperative transition shown by all FF domains (Table 1). The $\Delta G_{F\text{-}U}$ of FF-WT-OX measured by fluorescence and CD spectroscopy corresponds to $\approx$ 1.5 kcal/mol with a $[Urea]_{50\%}$ of $\approx$ 2 M, in contrast to the $\approx$ 5.0 kcal/mol and $[Urea]_{50\%}$ of $\approx$ 6 M exhibited by FF-WT. Reliable thermodynamic values could not be approximated for FF-R18A-OX since it unfolds at very low urea concentrations ($<$ 1 M). In FF-WT, $CySO_3H$ reduces $\Delta G_{F\text{-}U}$ by $\approx$ 3.5 kcal/mol. Because FF-R18A $\Delta G_{F\text{-}U} \approx$ 3.5 kcal/mol is not surprising that FF-R18A-OX is unstable even in the absence of denaturant.

Overall, thermal and chemical denaturation data, indicate that both oxidized domains are significantly destabilized relative to non-oxidized FF forms and that the impact of oxidation on the protein conformation depends on the initial stability of the native domain.

3.4. Dissecting the reasons behind oxidized FF domains destabilization

Whereas it is evident that the presence of a $CySO_3H$ at position 57 (supplementary Fig. 3A, B) impacts significantly the stability of FF domains, it is not clear if this effect results from the generic loss of the Cys57 residue or rather it is caused by the presence of the sulfonic acid in this specific position. In order to discriminate between these two possibilities, FF-WT Cys57 was mutated to both Ser and Asp. The Cys57Ser mutant (FF-C57S) was designed to investigate selectively the effect caused by the loss of the thiol group in the free Cys side chain (supplementary Fig. 3A, C). In the Cys57Asp mutant (FF-C57D), the aspartate is intended to act as a “cysteine sulfonic acid mimic”, emulating the negative charge of the oxidized Cys side chain (supplementary Fig. 3B, D). The changes in thermodynamic stability promoted by the mutations were predicted with the FoldX algorithm [22] ($\Delta\Delta G_{total} = \Delta G_{wt} - \Delta G_{mut}$), rendering $\Delta\Delta G$ values of -0.46 and 5.29 kcal/mol for the FF-C57S and FF-C57D mutants, respectively, thus anticipating that the previously observed domain destabilization was likely caused by the irreversible oxidation of Cys57 and not by the mere absence of its thiol group.

The secondary and tertiary structure of FF-C57S and FF-C57D mutants were analyzed by far-UV CD spectroscopy (supplementary Fig. 4A), Trp intrinsic fluorescence (supplementary Fig. 4B) and bis-ANS binding (supplementary Fig. 4C). The CD spectra of both FF mutants correspond to that of an α-helical structure (supplementary Fig. 4A). The increase in Trp intrinsic fluorescence emission recorded for FF-C57D suggests a certain opening of the globular structure as in the case of FF-WT-OX. In contrast, the FF-C57S Trp emission spectrum resembles that of FF-WT (supplementary Fig. 4B). The fluorescence emission of FF-C57D in the presence of bis-ANS confirms a certain exposure of hydrophobic regions to solvent, as in the case of FF-WT-OX. The FF-C57S mutant exhibits much lower bis-ANS binding, with a fluorescence intensity closer to that of FF-WT (supplementary Fig. 4C).

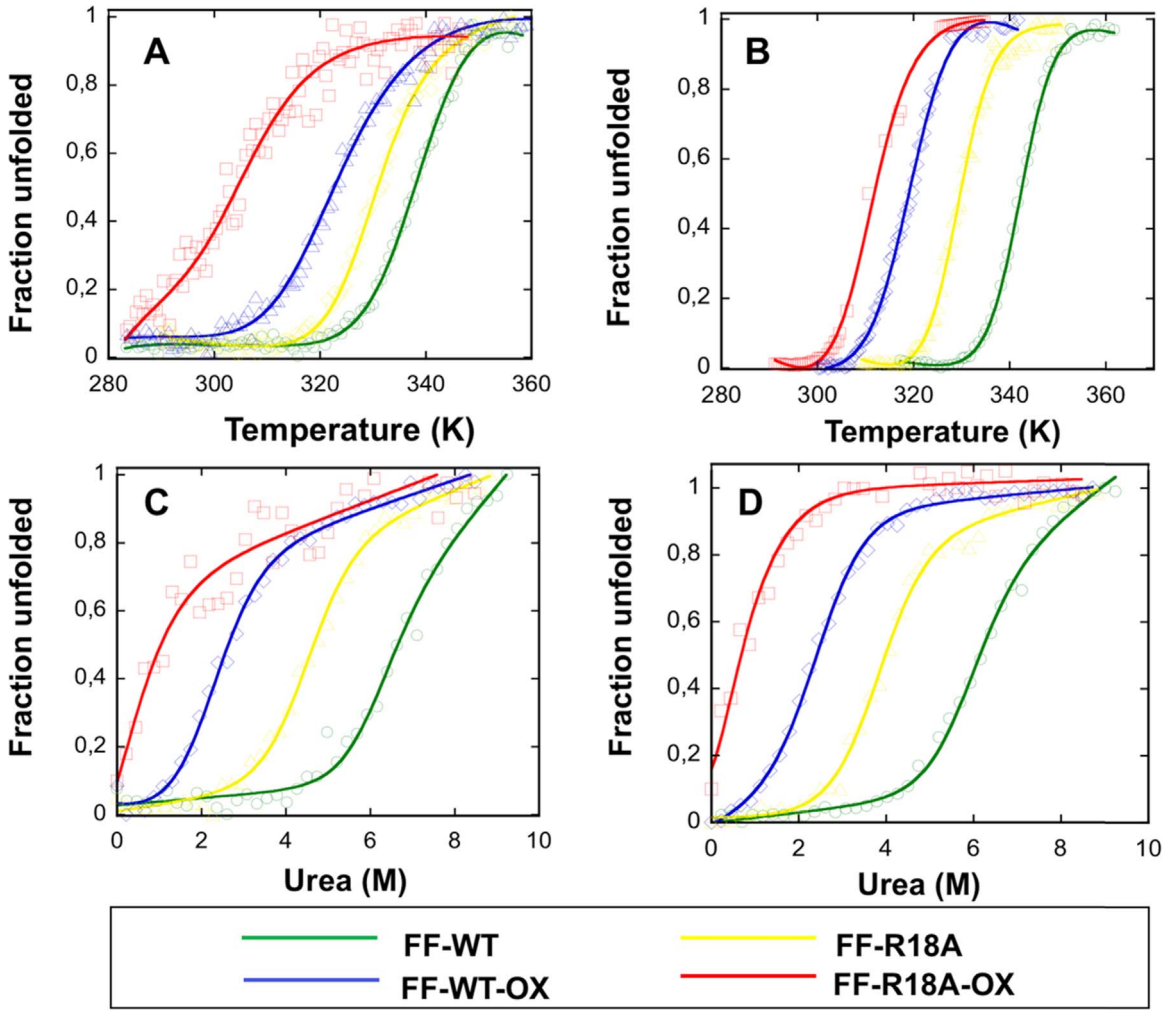

Fig. 3. *Thermal and chemical stabilities of FF domains.* Thermal stabilities were analyzed by (A) far-UV CD signal change at 222 nm and (B) Trp intrinsic fluorescence emission at 360 nm. Chemical equilibrium curves with urea were followed at 298 K by (C) far-UV CD at 222 nm and by (D) Trp intrinsic fluorescence at 360 nm.

Table 1
Thermodynamic properties of FF domains.

	[a]$\Delta G^{(H20)}$ (Kcal/mol)		[b]m (Kcal/mol·M)		[c][Urea] 50% (M)	
	CD	Trp intrinsic Fluorescence	CD	Trp intrinsic Fluorescence	CD	Trp intrinsic Fluorescence
FF-WT	5.14 ± 0.21	4.84 ± 0.08	0.80 ± 0.12	0.81 ± 0.01	6.42 ± 1.22	5.97 ± 0.17
FF-WT-OX	1.50 ± 0.11	1.67 ± 0.16	0.75 ± 0.07	0.80 ± 0.04	2.00 ± 0.33	2.08 ± 0.30
FF-R18A	3.39 ± 0.24	3.62 ± 0.32	0.75 ± 0.09	0.96 ± 0.19	4.52 ± 0.86	3.77 ± 1.07
FF-R18A-OX	–	–	–	–	–	–
FF-C57D	2.60 ± 0.09	2.46 ± 0.05	0.82 ± 0.04	0.74 ± 0.01	3.56 ± 0.28	3.32 ± 0.11
FF-C57S	4.43 ± 0.07	4.59 ± 0.07	0.77 ± 0.01	0.77 ± 0.02	5.75 ± 0.16	5.96 ± 0.24

[a] Gibbs energy of unfolding at [Urea] = 0.
[b] m value, dependence of free energy of unfolding with urea.
[c] The urea concentration required to unfold 50% of the protein molecules.

3.5. Thermal and chemical unfolding of FF Cys57 mutants

The thermal and chemical stability of FF Cys57 mutants was analyzed at pH 5.7. The resulting data were compared with the thermodynamic data obtained for FF-WT and FF-WT-OX (Fig. 4). Thermal and chemical denaturation were monitored by far-UV CD at 222 nm and by Trp fluorescence emission at 360 nm, respectively. A single cooperative transition that could be fitted to a two-state unfolding model was observed for both mutants. The melting temperatures obtained by CD and Trp intrinsic fluorescence are similar (Supplementary Table 3), coinciding to indicate that FF-C57D displays a thermal stability (T_m = 324 K) close to that of FF-WT-OX (T_m = 321 K), while FF-C57S (T_m = 335 K) is more similar to the wild type domain (T_m = 342 K). An analogous behaviour was observed in chemical unfolding, FF-C57D displaying a $\Delta G_{F\text{-}U} \approx 2.5$ kcal/mol and $[Urea]_{50\%} \approx 3.5$ M, whereas FF-C57S displays a $\Delta G_{F\text{-}U} \approx 4.5$ kcal/mol and $[Urea]_{50\%} \approx 5.9$ M (Table 1). Thus, taken together, these data indicate a similar destabilization and structural rearrangement for FF-C57D and FF-WT-OX, whereas the FF-C57S mutant, despite being slightly destabilized relative to FF-WT, is clearly more stable, in excellent agreement with the

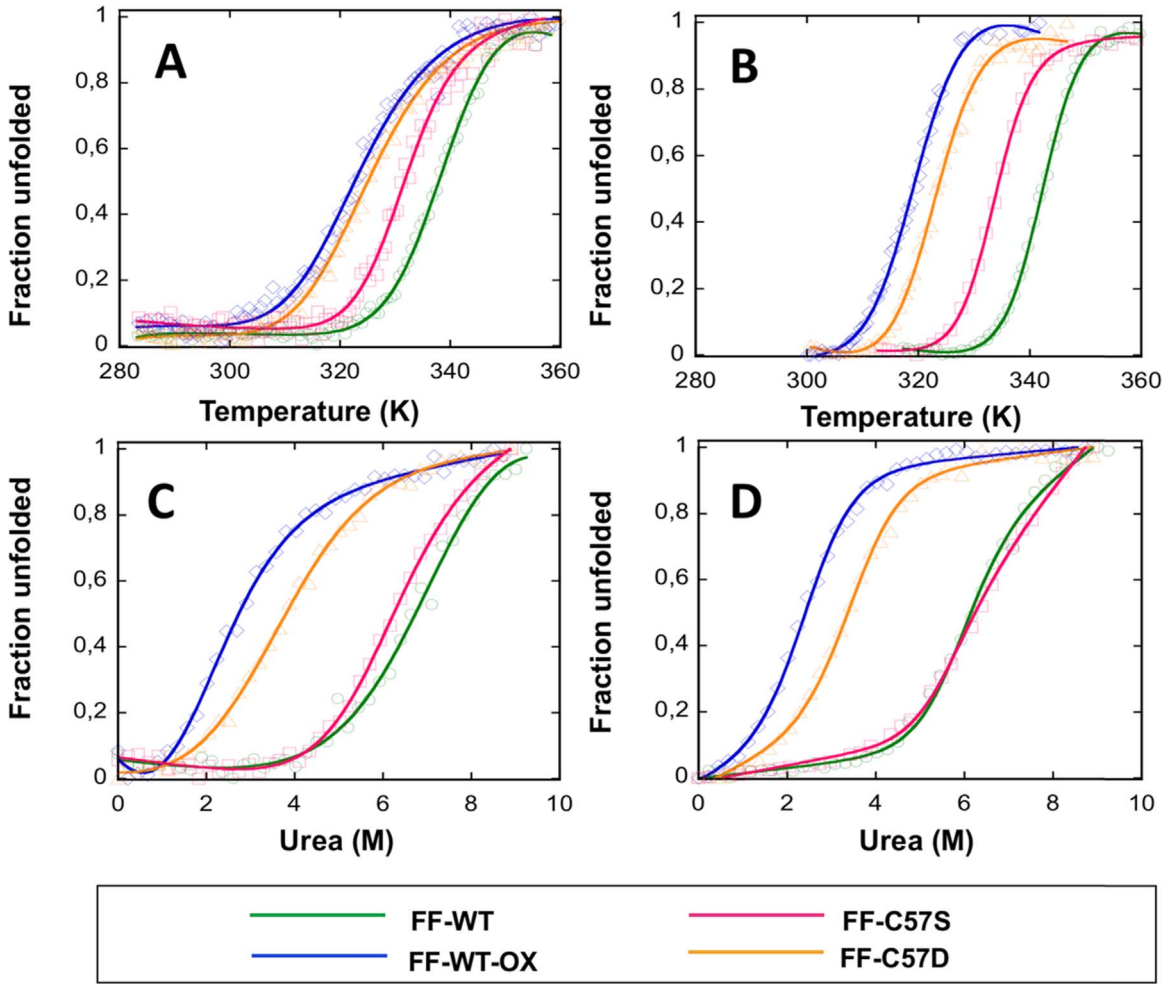

Fig. 4. *Thermal and chemical stabilities of FF cysteine mutants.* Thermal stabilities were measured by (A) far-UV CD signal change at 222 nm and (B) Trp intrinsic fluorescence emission at 360 nm. Chemical equilibrium curves with urea were monitored at 298 K by (C) far-UV CD at 222 nm and by (D) Trp intrinsic fluorescence at 360 nm.

computational predictions. The absence of Cys residues in the FF-C57S mutant allowed us to test whether the oxidation of Met3 could play a significant role in FF domains destabilization. Thermal denaturation of oxidized FF-C57S (FF-C57S-OX) indicates that modification of Met3 has a low impact on protein stability, since the its T_m is only 3 K lower than that of the non modified FF-C57S domain (Supplementary Fig. 5A and B and Supplementary Table 3).

3.6. Molecular dynamics (MD) simulations

We carried out molecular dynamics (MD) simulations to gain an atomistic description of the reasons behind FF-C57D destabilization. We used an enhanced sampling approach based on metadynamics that was demonstrated to be very accurate in describing the effects of point mutations or post-translational modification on protein conformation [24–26]. Metadynamics is a method that was developed to sample rare conformational transitions or post-translational modification on proteins and to estimate with high accuracy the associated free energy changes while keeping an atomistic description of both the solvent and the protein [27,28]. Metadynamics simulations were carried out with a state-of-the-art force field (CHARMM22*) [29] in explicit solvent for more than 400 ns, as well as extended up to 550 ns to ensure convergence of the free energy profiles. We used as reaction coordinates (collective variables) properties that account for the overall structures of the FF domain, i.e: the radius of gyration and the helical content in the three α-helices of the FF fold. In agreement with the experimental data, the C57D mutation has destabilizing effects in the metadynamics simulations. Indeed, it can be observed that the mutation induces the appearance of minima with larger Rg population in the free energy landscape of the protein (supplementary Fig. 6A), which also correlates with the destabilization of helix 1 (supplementary Fig. 6B) and specially helix 3, where Cys57 resides, (supplementary Fig. 6D), resulting in a lower helical content. According to MD, these changes in local helicity impact the solvent accessibility of the two Trp residues of the protein, in good agreement with the spectroscopic data.

3.7. Folding and unfolding kinetics of URN1 FF domains

Folding and unfolding kinetics of FF-WT, and FF-WT-OX, FF-C57S and FF-C57D domains, were followed by stopped-flow at pH 5.7 and 298 K under a wide range of denaturant conditions. For all domains, the folding and unfolding fluorescence traces fit well to a single exponential function. Chevron plots appear to be linear in the entire range of denaturant concentrations studied and fit well to a two-state model, indicating the absence of detectable intermediates (Fig. 5).

The rate constants for folding (K_f) and unfolding (K_u) and their dependence on the denaturant concentration (m_f and m_u) are shown in Table 2.

The FF-C57S mutant shows a folding rate very similar to that of FF-WT, displaying, however, a slightly faster unfolding rate. FF-WT-OX and FF-C57D domains fold only ≈3 times slower than FF-WT but, both domains unfold very fast, with 155 and 85 times faster unfolding rates than FF-WT, respectively. Thus, FF-WT-OX and FF-C57D domains display significantly reduced kinetic stability -the free energy difference

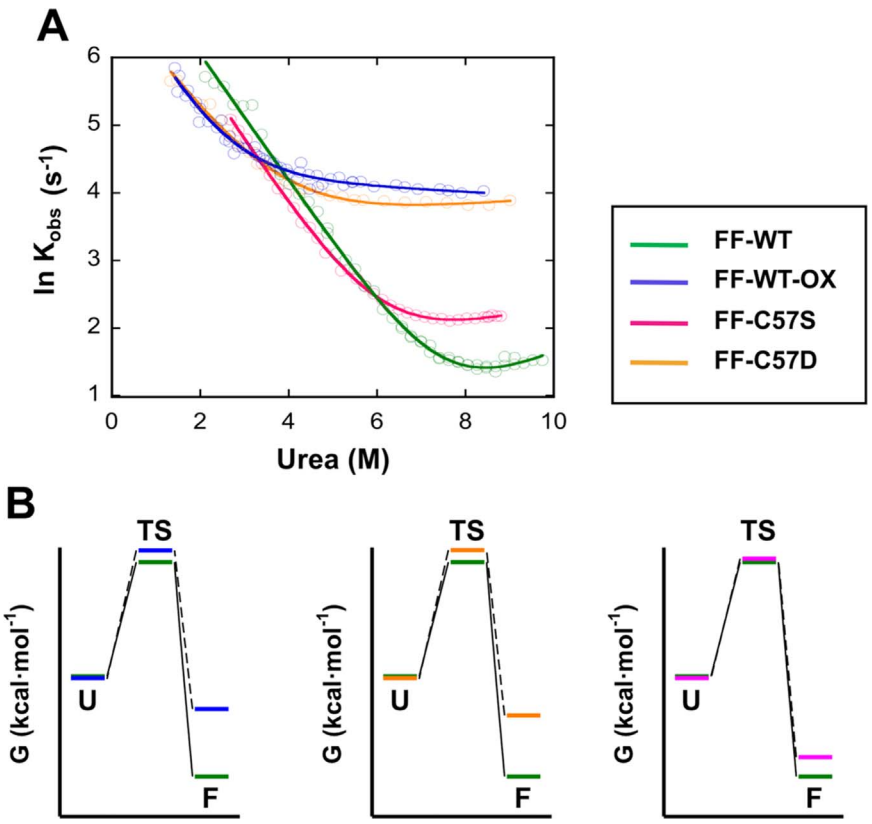

Fig. 5. *Folding kinetics of FF domains.* The kinetics of folding and unfolding were followed by Trp intrinsic fluorescence performing stopped-flow experiments at 298 K. A) Chevron plots are shown for the different domains. The rate constants were measured under conditions of apparent two-state folding. B) Schematic representation of the energy diagram for the folding process of the four FF domain variants, colors as in A).

between the native state and the unfolding transition state (Table 2 and Fig. 5), relative to the natural domain.

$\varphi_{F\text{-}U}$ values are used to map structures of protein-folding transition states from changes in free energies of denaturation and activation on mutation. A $\varphi_{F\text{-}U}$ value near 0 suggests that the region surrounding the mutation is unstructured in the transition state for folding, while a value near 1 indicates that the local structure around the mutation in the transition state closely resembles the structure in the native state. The $\varphi_{F\text{-}U}$ values of 0.17, 0.20 and 0.17 calculated for FF-WT-OX, FF-C57D and FF-C57S mutants, respectively, suggest that Cys57 is located in a region that is not significantly involved in the formation of the protein folding nucleus.

3.8. Amyloid fibril formation by FF domains

The aggregation kinetics of FF domains at 100 μM concentration were analyzed at pH 5.7 and 310 K following the changes over time in the fluorescence of the amyloid staining dye Thioflavin T (Th-T) binding (supplementary Fig. 7). We have shown that under these conditions WT-FF does not experience any detectable aggregation [18]. FF-WT-OX and FF-R18A-OX aggregation was very fast, displaying Th-T binding immediately after mixing. A similar behaviour is exhibited by the FF-C57D despite it required a longer time to attain the plateau. No significative Th-T binding was observed for FF-WT, FF-R18A and FF-C57S variants.

Thereafter, all FF domains were incubated at 50 μM concentration pH 5.7 and 310 K under agitation for one week in order to characterize the conformational, tinctorial and morphological properties of the aggregates (Fig. 6). Mature aggregates of both oxidized FF domains showed high Th-T binding. FF-WT did not show any significative Th-T binding, whereas FF-R18A exhibited certain dye binding, rendering, however, much lower fluorescence intensity than the oxidized FF domains (Fig. 6A). As in the case of FF-WT, the FF C57S mutant did not bind the amyloid dye. Conversely, FF-C57D induced high Th-T fluorescence (Fig. 6B). To confirm the nature of these aggregates we used another amyloid staining dye, Congo red (CR). In aggreeement with the Th-T binding data, the characteristic CR signal shift at ≈540 nm upon amyloid binding was observed for oxidized FF samples, while no CR binding was detected for FF-WT and FF-R18A solutions. FF-C57D bound the CR dye, promoting the same spectral change that FF-WT-OX. As expected, FF-C57S did not show CR binding. To assess whether aggregation involved a transition of the native α-helical structure into β-

Table 2
Folding kinetic parameters for FF domains.

	K_f (s^{-1})	K_u (s^{-1})	m *f* (Kcal/mol M)	m*u* (Kcal/mol M)	[a]m U-F (Kcal/mol M)	[b][ ]50% (M)	[c]ΔG *U-F* (Kcal/mol)	[d]ΔΔG *U-F* (Kcal/mol)	ΔΔG[d] *U-‡* (Kcal/mol)	ΔΔG[d] *F-‡* (Kcal/mol)
FF-WT	2819 ± 198	0.34 ± 0.12	0.94 ± 0.02	0.26 ± 0.04	0.71 ± 0.06	7.48	5.34	–	–	–
FF-WT-OX	976 ± 87	53.9 ± 1.4	0.98 ± 0.03	0.009 ± 0.003	0.58 ± 0.03	2.93	1.72	−3.63	0.63	−3.00
FF-C57D	946 ± 65	29.2 ± 0.9	0.89 ± 0.03	0.08 ± 0.01	0.57 ± 0.04	3.58	2.06	−3.28	0.65	−2.64
FF-C57S	2083 ± 76	1.45 ± 0.02	0.96 ± 0.01	0.20 ± 0.02	0.69 ± 0.03	6.26	4.31	−1.04	0.18	−0.86

[a] Dependence of the Gibbs energy of unfolding with urea.
[b] The urea concentration required to unfold 50% of the protein molecules.
[c] Gibbs energy of unfolding with urea determined from the kinetic parameters.
[d] The difference in free energy between the mutant protein and WT protein.

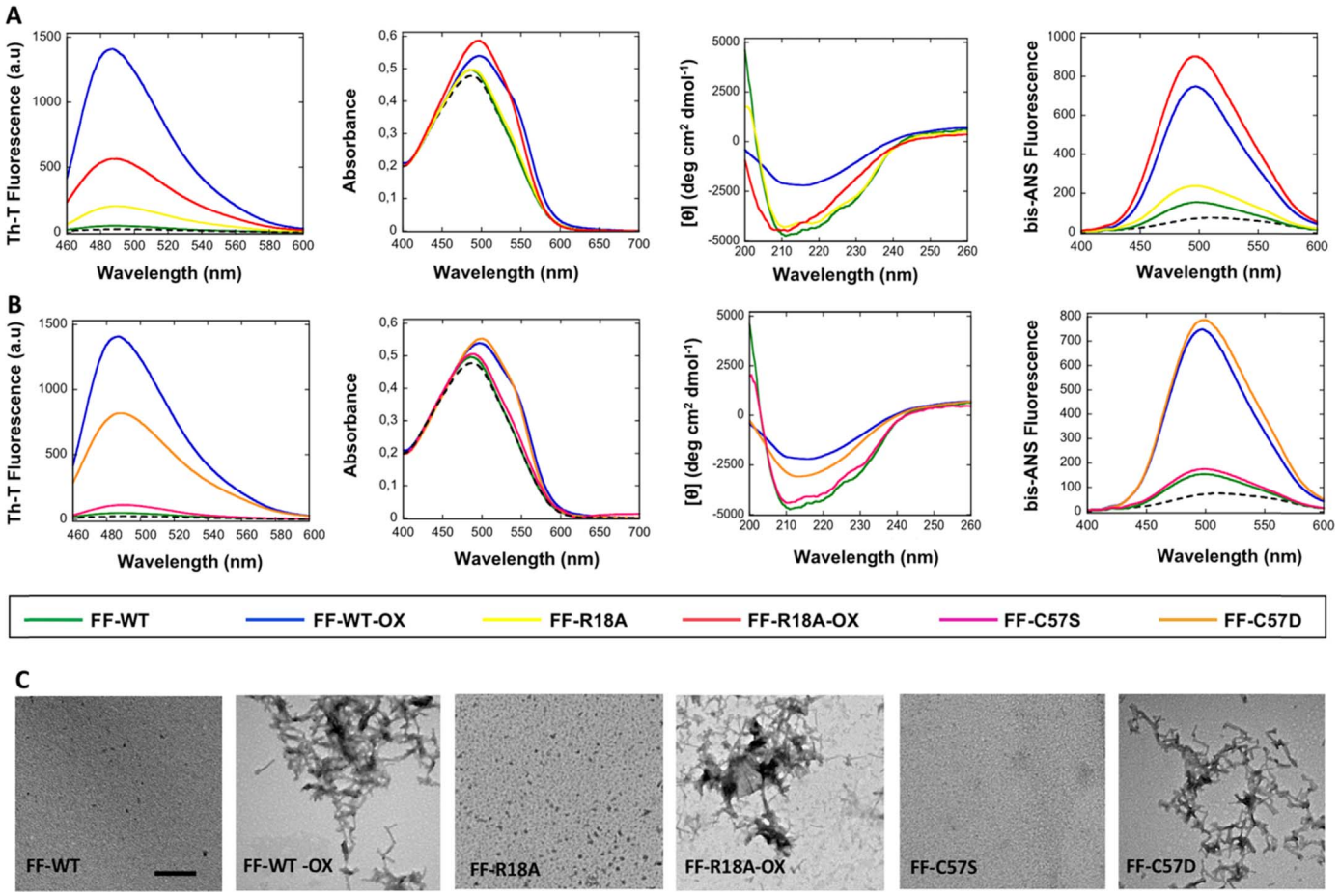

Fig. 6. *Conformational and morphological properties of URN1-FF aggregates at* pH 5.7. A) and B) FF domains were incubated at 310 K for one week and analyzed by measuring their Th-T fluorescence emission, Congo red binding, far-UV CD spectra and their binding to bis-ANS (from left to right). Free dyes are indicated with a dotted line. C) Representative micrographs of negatively stained FF aggregates visualized by TEM. The scale bar represents 500 nm.

sheet enriched conformations, the secondary protein structure of incubated solutions was monitored by far-UV CD spectroscopy. The presence of β-sheet structure was confirmed for FF-WT-OX as indicated by the typical minimum at ≈218 nm. FF-R18A OX also exhibited a CD spectrum compatible with the presence of β-sheet structures. Non-oxidized FF proteins displayed a α-helical native-like spectra. The FF-C57S also retained the native secondary structure whereas FF-C57D spectrum was dominated by a β-sheet component, resembling the FF-WT-OX spectrum. The bis-ANS binding to exposed hydrophobic regions was much higher in oxidized samples than in non-oxidized FF domains, indicaticave of intermolecular clustering of hydrophobic residues in the aggregated species. Again, FF-C57D displayed a bis-ANS binding very similar to that of FF-WT-OX, while the FF-C57S resembled FF-WT. Transmission Electron Microscopy (TEM) was used to assess the morphological properties of the aggregates (Fig. 6C). Both FF-WT-OX and FF-C57D formed short amyloid-like fibrils, while FF-R18A-OX displayed fibrillar structures combined with amorphous aggregates consistent with its very fast aggregation kinetics. On the other hand, scarce smaller size aggregates were detected for FF-R18A, while no recognizable aggregates were observed for FF-WT and FF-C57S. Oxidation of Met 3 in FF-C57S-OX had a negligible impact on aggregation as measured by Th-T and CR binding (Supplementary Fig. 5C and 5D).

Taken together, these data demonstrate that, under close to physiological conditions, irreversible oxidation of Cys57 promotes the formation of FF domain amyloid-like aggregates, highlighting the potential relevance of this type of PTM for *in vivo* proteostasis.

3.9. Large scale prediction of the effect of proteins free cysteines oxidation

The data reported above indicate that complete thiol oxidation to sulfonic acid at the single Cys residue in the FF domain induces conformational and structural changes that lead to the destabilization and aggregation of this small globular protein. This effect can be emulated by replacing Cys with Asp, which acts as a CysSO3H mimic, while the substitution by Ser, as expected, does not recapitulate the oxidation impact. In attempt to understand if site-specific Cys irreversible oxidation might represent a generic destabilization mechanism in natural proteins we used a database of 969 non-homologous protein structures containing Cys residues [30]. From the total 4136 Cys present in these proteins, 1446 are forming disulfide bonds and 2690 are free. Inspection of the respective structures indicated that 1338 of the non-disulfide-bonded Cys were solvent exposed. We virtually mutated all these residues into Asp or Ser residues using the FoldX algorithm [22] and calculated the predicted stability for every of the 2676 resulting mutants. The analysis revealed a clearly destabilizing effect of Asp mutations, with ΔΔG median value of 2.28 ± 0.10 kcal/mol (Fig. 7A). Cys to Ser mutations were predicted to have a much lower impact on stability with a ΔΔG median value of 0.92 ± 0.06 (95% CI, $p < 0.001$ T-student test). These results strongly suggest that the Cys oxidation destabilizing effect reported here for the FF protein model could occur in a wide number of physiologically relevant proteins. For example, the Cys to Asp mutants of human β-interferon (IFN-β) [31], and the human apoptosis regulator Bcl-xL [32] are predicted to be highly destabilized, with ΔΔG values of 4.57 and 6.38 kcal/mol, respectively.

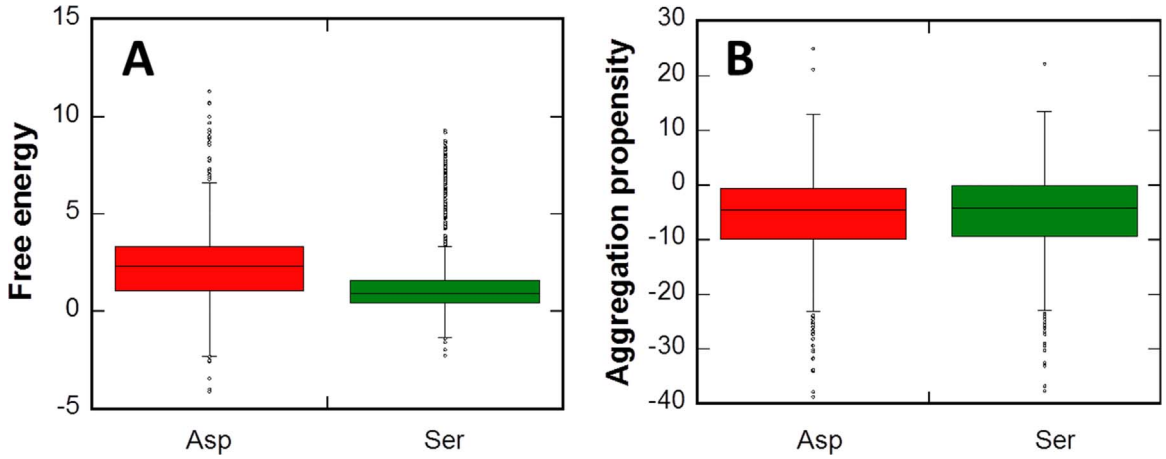

Fig. 7. *Stability and aggregation prediction in a large set of proteins with solvent exposed cysteine residues.* (A) Free and solvent exposed cysteines in a total of 969 non-homologous protein structures were virtually mutated into either aspartic or serine residues and the changes in overall stability, relative to the respective WT proteins, predicted using the FoldX algorithm. (B) The AGGRESCAN algorithm was used to calculate the aggregation propensity of the sequences of all these protein mutants.

The sequence-based aggregation prediction algorithms AGGRESCAN [33] and Zyggregator [34] were used to assess if Asp, and by analogy $CySO_3H$, might act creating new or stronger "hot spots" that favours the aggregation in the oxidized FF domain. No significant changes in the FF-C57S aggregation propensity were predicted, relative to FF-WT (supplementary Table 4). In contrast with the experimental data, a reduction of the aggregation propensity was predicted for the FF-C57D mutant, thus confirming that $CySO_3H$ induced aggregation owes to the impact this PTM exerts on the protein conformation. The AGGRESCAN analysis of the 2676 mutants modelled with FoldX predicted similar aggregation propensities for both Asp and Ser variants (Fig. 7B).

4. Discussion

Molecular aging, and particularly, the accumulation of oxidized proteins, are associated to a wide number of diseases, such as ALS, Alzheimer's disease, respiratory distress syndrome, muscular dystrophy, cataracts, rheumatoid arthritis and progeria [35]. Oxidation can promote alterations in the secondary, tertiary and quaternary structure of proteins [36–39]. The destabilized conformers resulting from protein oxidation might act as intermediates in the formation of amyloid assemblies in age-related disorders [40,41]. However, biophysical dissection of the contribution of individually modified amino acids to this deleterious conformational conversion is usually hampered by the simultaneous oxidation of different protein residues at different structural locations under oxidative conditions.

The data in the present work illustrate how the irreversible oxidation of a single Cys residue can cause dramatic changes in the folding landscape and aggregation properties of a globular protein. These results are consistent with the recent observation that the selective S-Glutathionylation of a Cys residue results in destabilization of titin immunoglobulin (Ig) domains [42]. We also show that the $CySO_3H$ destabilizing effect can be emulated by a Cys to Asp mutation. Contrary to FF-C57S, FF-C57D displays conformational, stability and aggregational features resembling those of the oxidized wild type protein, thus indicating that the main destabilizing effect comes from the acquisition of an additional negative charge and two bulky oxygens and not from the lack of the original free thiol, which is consistent with $CySO_3H$ being exclusively in a deprotonated form at physiological pH ($pKa < 2$). A similar impact on protein structure is expected for a milder Cys oxidation to a sulfinic acid ($pKa \sim 2$).

The use of MD simulations allowed us to study in atomistic detail the effect of the Asp mutation on the structural stability of the FF domain. In good agreement with the observed experimental decrease in stability, MD results indicate that the C57D mutation induces a significant local destabilization, affecting helix 1 and helix 3. We have previously shown that these helices comprise the most aggregation-prone regions in the FF domain, being able to lead its aggregation under destabilizing acidic conditions [18].

We were able to analyse, for the first time, the impact of $CySO_3H$ formation on the folding and unfolding rates of a globular protein, revealing that the conformational changes imposed by the sulfonic group do not affect significantly the folding rate. Accordingly, the φ values calculated for the oxidized FF protein and its two mutational variants are very close to 0, indicating that the C-terminal region does not present a native-like structure in the transition state for folding, as described for the homologous human HYPA/FBP11 FF domain [19]. The unfolding rate, however, is dramatically accelerated by the formation of the $CySO_3H$ or by the presence of the Asp residue. Thus, this site-specific PTM acts by significantly reducing the kinetic stability of the protein. Kinetic stability can be thought of as the average lifespan of a folded molecule between transient excursions to an unfolded state; thus, its reduction in the FF domain would allow for the transitory exposition of the aggregation-prone helices to the solvent.

The destabilization of the native state is a usual requirement for amyloid fibril formation in globular proteins [43]. Increasing evidences indicate that there may be a link between ROS-induced oxidative stress and the accumulation of misfolded proteins in the form of aggregates [44]. In particular, recent works suggest that Cys oxidation to sulfonic acid might be behind the aggregation of SOD1 in ALS or parkin in Parkinson disease [45,46]. We show here that $CySO_3H$ induced protein destabilization can promote the fast formation of amyloid-like insoluble aggregates under physiological conditions, without a need for global protein unfolding. Remarkably, our computational analysis suggests that a large number of unrelated proteins containing exposed free Cys residues are susceptible to suffer this deleterious conversion. Actually, the FF domain is a highly soluble, remarkably stable and fast folding protein. Despite all these properties confront aggregation, the oxidation of a single Cys residue suffices to promote its aggregation into amyloid fibrils. Many of the proteins in the cell do not exhibit these optimal features and indeed, according to the ProTherm database [47], most proteins would have stabilities < 3 kcal/mol and thus on the range of the FF-R18A domain (3.5 kcal/mol), for which Cys57 oxidation suffices to promote major conformational rearrangements leading to the rapid build up of aggregates. Overall, our data suggest that when ROS levels increase, as a result of aging or stress, cells might live on the edge of a proteostasis catastrophe, even if proteins are not extensively oxidized.

Acknowledgements

This work was funded by the Spanish Ministry of Economy and Competitiveness BIO2016-783-78310-R to S.V and by ICREA, ICREA-Academia 2015 to S.V. EP has been supported by a PRACE-DECI 13th GRANT on Archer (UK) and a Deic Pilot Gran ton Computerome (DK) to cover the computational resources needed for molecular simulations.

Conflict of interest

The authors declare that they have no competing interests.

Appendix A. Supporting information

Supplementary data associated with this article can be found in the online version at http://dx.doi.org/10.1016/j.redox.2017.10.022.

References

[1] G. Invernizzi, E. Papaleo, R. Sabate, S. Ventura, Protein aggregation: mechanisms and functional consequences, Int. J. Biochem. Cell Biol. 44 (2012) 1541–1554.
[2] F. Chiti, C.M. Dobson, Protein Misfolding, Functional Amyloid, and Human Disease, Annu. Rev. Biochem. 75 (2006) 333–366.
[3] E. Monsellier, F. Chiti, Prevention of amyloid-like aggregation as a driving force of protein evolution, EMBO Rep. 8 (2007) 737–742.
[4] S.M. Johnson, R.L. Wiseman, Y. Sekijima, N.S. Green, S.L. Adamski-Werner, J.W. Kelly, Native state kinetic stabilization as a strategy to ameliorate protein misfolding diseases: a focus on the transthyretin amyloidoses, Acc. Chem. Res. 38 (2005) 911–921.
[5] T. Poshusta, N. Katoh, M. Gertz, A. Dispenzieri, M. Ramirez-Alvarado, Thermal stability threshold for amyloid formation in light chain amyloidosis, Int. J. Mol. Sci. 14 (2013) 22604–22617.
[6] A. Espargaró, V. Castillo, N.S. de Groot, S. Ventura, The in vivo and in vitro aggregation properties of globular proteins correlate with their conformational stability: the SH3 case, J. Mol. Biol. 378 (2008) 1116–1131.
[7] F. Chiti, C.M. Dobson, Amyloid formation by globular proteins under native conditions, Nat. Chem. Biol. 5 (2009) 15–22.
[8] M.P. Murphy, How mitochondria produce reactive oxygen species, Biochem. J. 417 (2009) 1–13.
[9] I.V.J. Murray, L. Liu, H. Komatsu, K. Uryu, G. Xiao, J.A. Lawson, P.H. Axelsen, Membrane-mediated amyloidogenesis and the promotion of oxidative lipid damage by amyloid beta proteins, J. Biol. Chem. 282 (2007) 9335–9345.
[10] D.A. Bosco, D.M. Fowler, Q. Zhang, J. Nieva, E.T. Powers, P. Wentworth, R.A. Lerner, J.W. Kelly, Elevated levels of oxidized cholesterol metabolites in Lewy body disease brains accelerate α-synuclein fibrilization, Nat. Chem. Biol. 2 (2006) 249–253.
[11] E.R. Stadtman, R.L. Levine, Protein oxidation, Ann. N. Y. Acad. Sci. 899 (2000) 191–208.
[12] M. Hamann, T. Zhang, S. Hendrich, J.A. Thomas, Quantitation of protein sulfinic and sulfonic acid, irreversibly oxidized protein cysteine sites in cellular proteins, Methods Enzymol. 348 (2002) 146–156.
[13] M.T. Bedford, P. Leder, The FF domain: a novel motif that often accompanies WW domains, Trends Biochem. Sci. 24 (1999) 264–265.
[14] R. Bonet, X. Ramirez-Espain, M.J. Macias, Solution structure of the yeast URN1 splicing factor FF domain: comparative analysis of charge distributions in FF domain structures-FFs and SURPs, two domains with a similar fold, Proteins 73 (2008) 1001–1009.
[15] M. Allen, A. Friedler, O. Schon, M. Bycroft, The structure of an FF domain from human HYPA/FBP11, J. Mol. Biol. 323 (2002) 411–416.
[16] W. Jiang, R. Sordella, G.-C. Chen, S. Hakre, A.L. Roy, J. Settleman, An FF domain-dependent protein interaction mediates a signaling pathway for growth factor-induced gene expression, Mol. Cell. 17 (2005) 23–35.
[17] M.J. Smith, S. Kulkarni, T. Pawson, FF domains of CA150 bind transcription and splicing factors through multiple weak interactions, Mol. Cell. Biol. 24 (2004) 9274–9285.
[18] V. Castillo, F. Chiti, S. Ventura, The N-terminal helix controls the transition between the soluble and amyloid states of an FF domain, PLoS One 8 (2013) e58297.
[19] P. Jemth, R. Day, S. Gianni, F. Khan, M. Allen, V. Daggett, A.R. Fersht, The Structure of the Major Transition State for Folding of an FF Domain from Experiment and Simulation, J. Mol. Biol. 350 (2005) 363–378.
[20] D.M. Korzhnev, T.L. Religa, L.E. Kay, Transiently populated intermediate functions as a branching point of the FF domain folding pathway, Proc. Natl. Acad. Sci. 109 (2012) 17777–17782.
[21] D.M. Korzhnev, T.L. Religa, W. Banachewicz, A.R. Fersht, L.E. Kay, A. Transient, and Low-Populated Protein-Folding Intermediate at Atomic Resolution, Sci. (80-.) 329 (2010) 1312–1316.
[22] J. Schymkowitz, J. Borg, F. Stricher, R. Nys, F. Rousseau, L. Serrano, The FoldX web server: an online force field, Nucleic Acids Res. 33 (2005) W382–W388.
[23] R. Guerois, J.E. Nielsen, L. Serrano, Predicting Changes in the Stability of Proteins and Protein Complexes: a Study of More Than 1000 Mutations, J. Mol. Biol. 320 (2002) 369–387.
[24] E. Papaleo, L. Sutto, F.L. Gervasio, K. Lindorff-Larsen, Conformational changes and free energies in a proline isomerase, J. Chem. Theory Comput. 10 (2014) 4169–4174.
[25] G. Saladino, F.L. Gervasio, Modeling the effect of pathogenic mutations on the conformational landscape of protein kinases, Curr. Opin. Struct. Biol. 37 (2016) 108–114.
[26] M. Lambrughi, L. De Gioia, F.L. Gervasio, K. Lindorff-Larsen, R. Nussinov, C. Urani, M. Bruschi, E. Papaleo, DNA-binding protects p53 from interactions with cofactors involved in transcription-independent functions, Nucleic Acids Res. 44 (2016) 9096–9109.
[27] V. Spiwok, Z. Sucur, P. Hosek, Enhanced sampling techniques in biomolecular simulations, Biotechnol. Adv. 33 (2015) 1130–1140.
[28] A. Laio, F.L. Gervasio, Metadynamics: a method to simulate rare events and reconstruct the free energy in biophysics, chemistry and material science, Rep. Prog. Phys. 71 (2008) 126601.
[29] S. Piana, K. Lindorff-Larsen, D.E. Shaw, How robust are protein folding simulations with respect to force field parameterization? Biophys. J. 100 (2011) L47–L49.
[30] P.L. Martelli, P. Fariselli, L. Malaguti, R. Casadio, Prediction of the disulfide bonding state of cysteines in proteins with hidden neural networks, Protein Eng. 15 (2002) 951–953.
[31] L.H. Kasper, A.T. Reder, Immunomodulatory activity of interferon-beta, Ann. Clin. Transl. Neurol. 1 (2014) 622–631.
[32] D. Hockenbery, G. Nuñez, C. Milliman, R.D. Schreiber, S.J. Korsmeyer, Bcl-2 is an inner mitochondrial membrane protein that blocks programmed cell death, Nature 348 (1990) 334–336.
[33] O. Conchillo-Solé, N.S. de Groot, F.X. Avilés, J. Vendrell, X. Daura, S. Ventura, AGGRESCAN: a server for the prediction and evaluation of “hot spots” of aggregation in polypeptides, BMC Bioinforma. 8 (2007) 65.
[34] G.G. Tartaglia, M. Vendruscolo, The Zyggregator method for predicting protein aggregation propensities, Chem. Soc. Rev. 37 (2008) 1395–1401.
[35] B.S. Berlett, E.R. Stadtman, Protein oxidation in aging, disease, and oxidative stress, J. Biol. Chem. 272 (1997) 20313–20316.
[36] R.T. Dean, S. Fu, R. Stocker, M.J. Davies, Biochemistry and pathology of radical-mediated protein oxidation, Biochem. J. 324 (1997) 1–18.
[37] A. Milzani, R. Rossi, P. Di Simplicio, D. Giustarini, R. Colombo, I. DalleDonne, The oxidation produced by hydrogen peroxide on Ca-ATP-G-actin, Protein Sci. 9 (2000) 1774–1782.
[38] P. Lasch, T. Petras, O. Ullrich, J. Backmann, D. Naumann, T. Grune, Hydrogen Peroxide-induced Structural Alterations of RNase A, J. Biol. Chem. 276 (2001) 9492–9502.
[39] X. Zhou, C. Mester, P.M. Stemmer, G.E. Reid, Oxidation-Induced Conformational Changes in Calcineurin Determined by Covalent Labeling and Tandem Mass Spectrometry, Biochemistry 53 (2014) 6754–6765.
[40] T.C. Squier, Oxidative stress and protein aggregation during biological aging, Exp. Gerontol. 36 (2001) 1539–1550.
[41] R.A. Dunlop, U.T. Brunk, K.J. Rodgers, Oxidized proteins: mechanisms of removal and consequences of accumulation, IUBMB Life. 61 (2009) 522–527.
[42] J. Alegre-Cebollada, P. Kosuri, D. Giganti, E. Eckels, J.A. Rivas-Pardo, N. Hamdani, C.M. Warren, R.J. Solaro, W.A. Linke, J.M. Fernández, S-glutathionylation of cryptic cysteines enhances titin elasticity by blocking protein folding, Cell 156 (2014) 1235–1246.
[43] F. Chiti, P. Webster, N. Taddei, A. Clark, M. Stefani, G. Ramponi, C.M. Dobson, Designing conditions for in vitro formation of amyloid protofilaments and fibrils, Proc. Natl. Acad. Sci. USA 96 (1999) 3590–3594.
[44] E. Bossy-Wetzel, R. Schwarzenbacher, S.A. Lipton, Molecular pathways to neurodegeneration, Nat. Med. 10 (2004) S2–S9.
[45] J. Choi, H.D. Rees, S.T. Weintraub, A.I. Levey, L.-S. Chin, L. Li, Oxidative modifications and aggregation of Cu,Zn-superoxide dismutase associated with alzheimer and parkinson diseases, J. Biol. Chem. 280 (2005) 11648–11655.
[46] F. Meng, D. Yao, Y. Shi, J. Kabakoff, W. Wu, J. Reicher, Y. Ma, B. Moosmann, E. Masliah, S.A. Lipton, Z. Gu, Oxidation of the cysteine-rich regions of parkin perturbs its E3 ligase activity and contributes to protein aggregation, Mol. Neurodegener. 6 (2011) 34.
[47] K.A. Bava, M.M. Gromiha, H. Uedaira, K. Kitajima, A. Sarai, ProTherm, version 4.0: thermodynamic database for proteins and mutants, Nucleic Acids Res. 32 (2004) D120–D121.